atmosphere

MDPI

Article

Comparison of Ionospheric Response to Two Types of Electron Concentration Disturbances

Artur F. Yakovets [1], Galina I. Gordiyenko [1,*], Olga N. Kryakunova [1] and Yurii G. Litvinov [2]

[1] Institute of the Ionosphere, Joint-Stock Company "National Center for Space Research and Technology", Almaty 050010, Kazakhstan; yakovets@ionos.kz (A.F.Y.); kryakunova@ionos.kz (O.N.K.)
[2] Joint-Stock Company "Academy of Civil Aviation", Almaty 050039, Kazakhstan; litvinov@ionos.kz
* Correspondence: ggordiyenko@mail.ru or ggordiyenko@ionos.kz

Abstract: Based on the data of vertical sounding of the ionosphere in Almaty in 2000–2008, the paper deals with the response of the *F*2-layer to the passage of large-scale traveling ionospheric disturbances (LSTIDs) and the formation of the nighttime enhancements in the electron concentration of the *F*2-layer. For these two types of perturbations, we compared behavior in the time of the following layer parameters: the height of maximum of the layer (h_mF), the height of the bottom of the layer ($h_{bot}F$), the half-thickness of the layer ($\Delta h = h_mF - h_{bot}F$), the electron concentration at fixed heights and at the maximum of the layer (N_mF), the height profiles of the nighttime enhancement peak-to-peak value of the *F*2-layer (A), and the height h_{Am} corresponding to the maximum enhancement amplitude. The parameters h_mF, $h_{bot}F$ and Δh demonstrate similar dependences associated with the temporal expansion and upward rise of the ionospheric layer and its lowering, accompanied by layer compression, giving an N_mF peak at the moment of maximum compression. The common features of the profiles of two types of disturbances are found: the height h_{Am} is always below h_mF, there is a good correlation between h_{Am} and h_mF, and the difference between h_{Am} and h_mF increases linearly with h_mF.

Keywords: vertical sounding of the ionosphere; large-scale traveling ionospheric disturbances; nighttime enhancements in the electron concentration of the *F*2-layer

Citation: Yakovets, A.F.; Gordiyenko, G.I.; Kryakunova, O.N.; Litvinov, Y.G. Comparison of Ionospheric Response to Two Types of Electron Concentration Disturbances. *Atmosphere* **2022**, *13*, 602. https://doi.org/10.3390/atmos13040602

Academic Editors: Goderdzi Didebulidze and Sergey P. Kshevetskii

Received: 10 March 2022
Accepted: 7 April 2022
Published: 9 April 2022

1. Introduction

There is a large class of disturbances in the *F*2-layer of the ionosphere, which are superimposed on regular diurnal variations in the electron concentration. Different types of perturbations are characterized by different physical mechanisms of their generation. Medium- and large-scale traveling ionospheric disturbances (MSTIDs and LSTIDs) are apparently the most characteristic features of the inhomogeneous structure of the ionosphere. Large-scale traveling ionospheric disturbances are a manifestation of the propagation of atmospheric gravity waves (AGWs) in the ionospheric plasma [1,2]. The results of theoretical and experimental studies of the propagation of AGWs in a neutral atmosphere and their ionospheric manifestations are summarized in a number of review papers [1,3].

Another type of ionospheric disturbances is nighttime enhancements in the electron concentration of the ionospheric *F*2-layer. This type of disturbances is described in numerous papers [4–8], in which, along with the morphology of the phenomenon, the mechanism of its formation is considered, including: (a) ambipolar diffusion of ionospheric plasma; (b) plasma drift along magnetic field lines due to meridional neutral wind; (c) plasma exchange between the plasmasphere and ionosphere; and (d) recombination.

Another type is *F*2-layer disturbances under quiet geomagnetic conditions (*Q*-disturbances), whose morphology was described in [9]. The mechanisms of their formation depend on the latitude. At middle latitudes, *Q*-disturbances can be generated by meteorological sources [10]. Note, that the duration of the existence of the listed types of perturbations takes approximately

the same time interval from several tens of minutes to several hours. In addition, LSTIDs and nighttime enhancements are observed with a high probability exceeding tens of percent [6,7,11].

For the first time, Lynn et al. [12] described common features in the behavior of the electron concentration, *F*2-layer maximum height, and layer half-thickness (N_mF, h_mF, and Δh) for three types of ionospheric disturbances of different nature. The first type represented medium- and large-scale TIDs. The second type represented perturbations occurring at night at equatorial latitudes associated with the $\mathbf{E} \times \mathbf{B}$ plasma drift and the midnight collapse of h_mF. The third type represented the recently revealed [13] disturbances at mid-latitudes of the southern hemisphere, which take place in the morning and afternoon hours of the equinox months. Disturbances of this type are associated with tidal variations in the atmosphere. Lynn et al. [12] showed that, despite the different physical mechanisms of generation of ionospheric disturbances, the responses of the *F*2-layer parameters demonstrate the same features: upward movement and simultaneous expansion of the layer, then its subsequent downward movement, including layer compression, which leads to the formation of the maximum value of the electron concentration at the height of the layer maximum at the moment of the greatest compression. Then, the authors conclude that the compression and expansion of the ionosphere is probably the dominant cause of the formation of electron concentration disturbances under the quiet geomagnetic conditions.

The aim of this paper is to verify the concept of Lynn et al. [12] on the examples of disturbances associated with the propagation of LSTIDs and the formation of nighttime enhancements. This paper is organized as follows. Observation equipment and methods for processing ionograms are described in Section 2. Results and discussion are described in Section 3. Variations in ionospheric parameters during the passage of the LSTIDs are described in Section 3.1. Variations in ionospheric parameters during the formation of nighttime enhancements are described in Section 3.2. Altitude profiles of LSTID amplitudes and nighttime enhancements are described in Section 3.3.

2. Instrumentation and Data Processing Method

Ionosphere observations are carried out at the Institute of the Ionosphere (Almaty, Kazakhstan (76°55′ E, 43°15′ N)) on a digital ionosonde PARUS (http://www.izmiran.rssi.ru, accessed on 10 March 2022) connected to a computer, which is designed to collect, store and process ionograms. Information is read from ionograms by a semi-automatic method. The ionosonde collects data with 5 min cadence. The duration of observation sessions, depending on the season, is 10–14 h, while the middle of the session coincides with local midnight. During the analyzed period, 1166 observation sessions were carried out. Primary processing of ionograms includes reading the values of the virtual heights ($h'(t)$) of the radio signal reflection at a number of fixed operating frequencies of sounding and the values of the ordinary (f_oF) and extraordinary (f_xF) critical frequencies. The ionosonde provides reading accuracy $h'(t) \approx 2.5$ km and reading accuracy $f_oF \approx 0.05$ MHz. In this paper, sounding data for the period 2001–2008 are analyzed. The distance between adjacent operating frequencies was chosen to be 0.5 MHz in order to obtain a sufficiently detailed height profile of $h'(t)$ variations. Further processing included obtaining $N(h)$ profiles from ionograms using the POLAN program [14] for converting virtual heights into true heights. In this method, the $N(h)$-profile is approximated by overlapping polynomials, while the section of the profile near *NmF* is approximated by a parabola. To obtain quantitative estimates of the LSTID parameters and nighttime enhancements in the electron concentration of the *F*2-layer, we built the behavior of the electron concentration at a number of fixed heights (the distance between neighboring heights was 10 km), as well as the time variations of h_mF, $h_{bot}F$, Δh, and the critical frequency (f_oF) for the ordinary reflected signal components. The critical frequency of the layer (in MHz) is related to the electron concentration at the layer maximum (N_mF), expressed as the number of electrons per cubic centimeter, by the relation $N_mF = 1.24 \times 10^4 \, (f_oF)^2$. The height corresponding to the electron concentration at the level of $0.3N_mF$ was taken as the height of the layer bottom. The coefficient 0.3 was selected empirically from the point of view of the closest approximation of this height to the height

at which a significant height gradient of the electron concentration was observed in the experimental $N(h)$ profiles.

3. Results and Discussion

3.1. Traveling Ionospheric Disturbances

A visual review of the processed data showed that a significant part (about half) of the experimental time series obtained by us was characterized by quasi-periodic variations in ionospheric parameters. As an example, Figure 1 illustrates variations in the critical frequencies of the ordinary and extraordinary components (f_oF and f_xF) (a), variations in the virtual heights $h'(t)$ for the extraordinary component on a series of probing frequencies indicated near the corresponding variations (b), variations in the electron concentration on a series of fixed heights and at the maximum of the $F2$-layer (thick curve) (c), variations in the h_mF, $h_{bot}F$, ΔhF, and f_oF (d). The quasi-periodic variations of parameters of the $F2$-layer shown in the figure can be associated with a large geomagnetic storm with a sudden onset that began on 24 July 2004 at 06:00 UT.

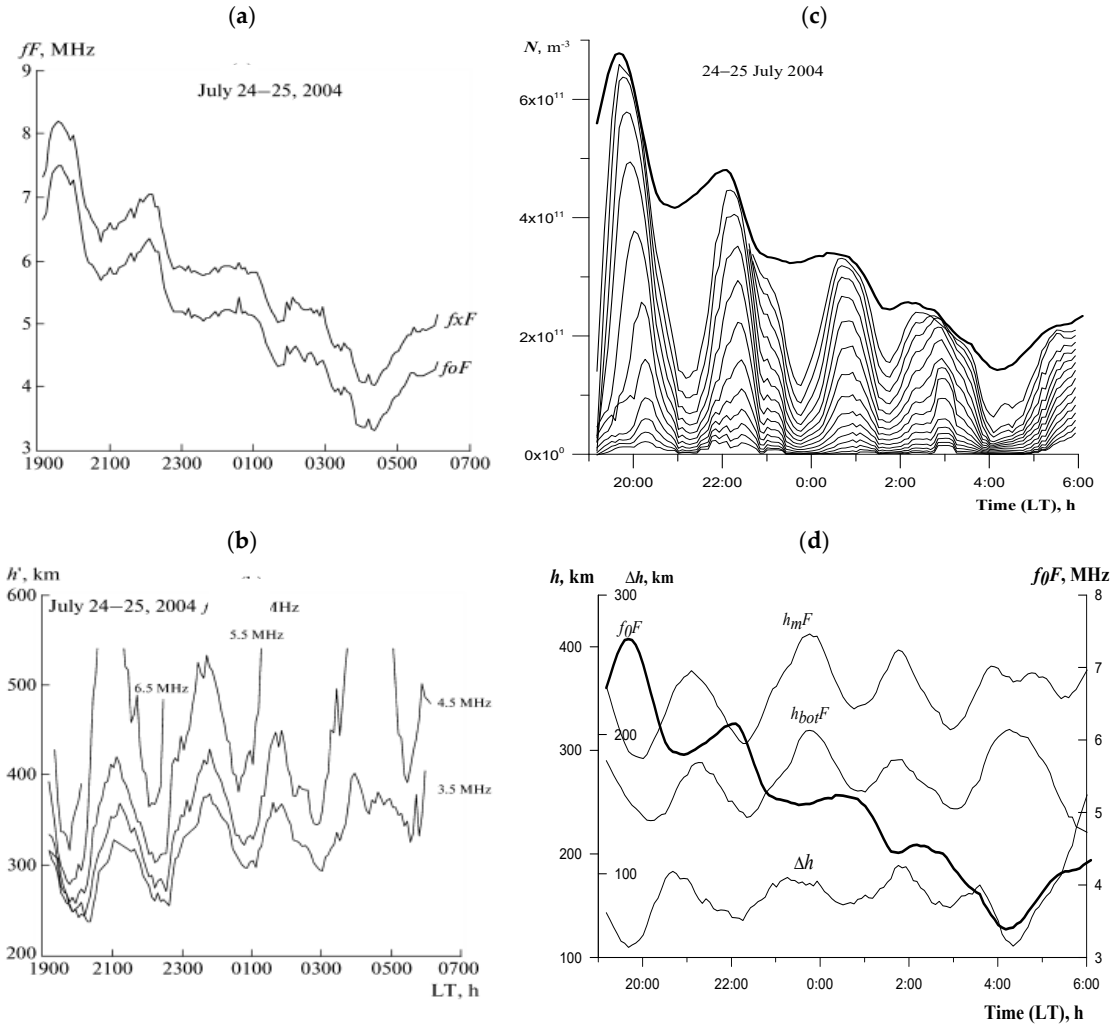

Figure 1. Variations f_oF and f_xF (**a**), $h'(t)$ at a series of probing frequencies (**b**), electron concentration N at a series of fixed heights and at the maximum of the $F2$-layer (thick curve) (**c**), heights h_mF, $h_{bot}F$, Δh and f_oF (**d**).

During geomagnetic storms [1], polar electrojets are rapidly enhanced, which leads to local heating of the atmosphere. The process of rapid expansion and subsequent compression of the atmosphere creates large-scale atmospheric gravity waves (LSAGWs) propagat-

ing towards the equator and generating LSTIDs on their way. It follows from the figure that, against the background of their gradual decrease due to the usual diurnal variation of the electron concentration at the maximum of the *F*2-layer, the critical frequencies exhibit quasi-periodic variations with a period of ~140 min. Pronounced variations with the same period are also observed in the behavior of $h'(t)$. It can be seen that, from the series of $h'(t)$ variations shown in the figure, only the lower curve is present during the entire eleven-hour observation session. Due to the change in the value of the critical frequency of the layer during the night, higher operating frequencies at one time or another turned out to be greater than the critical frequency of the layer, and reflections at these frequencies disappeared. The $h'(t)$ variation records shown in the figure contain features characteristic of most measurement sessions in which quasi-periodic variations in ionospheric parameters were observed. Let us consider these features. The amplitude of variations $h'(t)$ increases with the increase in the probing frequency and, consequently, the height of the radio signal reflection. The figure also shows that the variations in $h'(t)$ at lower frequencies lag behind the variations at higher frequencies. Two conclusions follow from this. Firstly, the fact that $h'(t)$ variations at fixed frequencies arise as a result of the passage of waves and, secondly, that these waves are internal gravity waves, which are characterized by opposite directions of group and phase velocities in the vertical plane. It is known that the AGW energy is transferred to the thermosphere from the lower layers of the ionosphere; therefore, the motion of the AGW phase front must be directed from top to bottom, which is observed in the figure.

Figure 1c illustrates the smoothed variations of the ionospheric electron concentration ($N(t)$) for the considered night at a series of heights. The lower curve corresponds to the height of the layer bottom (h_{bot} = 190 km). The upper (thick) curve corresponds to variations in $N_m(t)$ at the maximum of the *F*2-layer. To eliminate high-frequency components, both of ionospheric origin and those caused by noise arising during processing, low-frequency filtering of the series was carried out using a sliding window with a length T = 60 min. An analysis of the phase relationships between the variation peaks in f_oF, h_mF, $h_{bot}F$, Δh shown in Figure 1d gives the following results. Peaks of variations in f_oF (and, consequently, electron concentration) occur when the true height of the *F*2-layer maximum decreases and at the same time, when the half-thickness of the *F*2-layer reaches a minimum, i.e., at the moment of maximum compression of the ionosphere. An explanation of the phase relationships between variations of ionospheric parameters is given in [15]. The given phase relationships between the considered layer parameters (f_oF2, h_mF, $h_{bot}F$, Δh) are also preserved for other observation sessions with intense wave activity, for which time variations of these parameters were built.

The physical processes that occur in the ionosphere when an AGW passes through it were studied using the model of Millward et al. [16]. The AGW generated in the polar region, when it reaches middle latitudes, has a wavelength exceeding 1000 km. For such a wave, the movement of neutral gas at the heights of the *F*2-layer represents a horizontal wind blowing along the meridian to the south during the passage of the positive half-wave over the observation site and to the north during the passage of the negative half-wave over the observation site. Since the *F*2-layer of the ionosphere is a weakly ionized plasma, it is involved in motion due to collisions of neutrals with ions.

In the *F*2-layer, the ionospheric plasma is magnetized, so that its motion is possible only along the magnetic field tubes. The speed of this motion is determined by the neutral wind component directed along the magnetic field. The neutral wind generated successively by positive and negative half-waves forces the plasma to move up and down along the magnetic field lines, respectively, leading to periodic oscillations in the height of the *F*2-layer maximum.

Based on the nature of variations in the main parameters of the *F*2-layer of the ionosphere, presented in Figure 1d, one can describe a qualitative picture of the behavior of the electron concentration in the F2-layer during the passage of the AGW. A common characteristic of AGWs is that their amplitude increases with altitude. Consequently, the

value of the horizontal velocity of transfer of neutral particles in the AGW, which causes TID, increases with height. Consider a half-wave, in which the particles move along the meridian to the south. The movement of neutral particles causes charged particles to move upward along geomagnetic field lines to higher altitudes. Additionally, since the amplitude of the wave increases with height, the plasma at high altitudes will move up a greater distance compared to the plasma that was originally at a lower altitude. Therefore, as a result, an increase in the layer thickness and a decrease in the electron concentration at the layer maximum will be observed. The next AGW half-wave with particles moving to the north will lead to the opposite picture: the *F*2-layer starts moving down to lower heights. Its thickness will decrease as the ionization concentration at the layer maximum increases. This is how the process of periodic redistribution of the ionospheric plasma over the changing thickness of the layer takes place, while the integral content of the ionosphere remains close to a constant value during the wave period, if the changes associated with the diurnal variation are not taken into account.

3.2. Night Enhancement in F2-Layer Electron Concentration

The probability of formation of nighttime enhancements is very high. On average, it reaches 50%, and in the winter months it can exceed 80% [4,6]. We used the Dst index to assess the geomagnetic activity. The value Dst = 7 shown in Figure 2a represented the maximum value of the index, which occurred in the time interval starting several hours before the beginning of the recorded enhancement in the electron concentration and ending at the end of the enhancement. The choice of the boundaries of the interval for estimating the value of geomagnetic activity, which can be related to the observed phenomenon, is determined by the fact that the usual propagation time of disturbances from polar to middle latitudes is ~2–3 h [1].

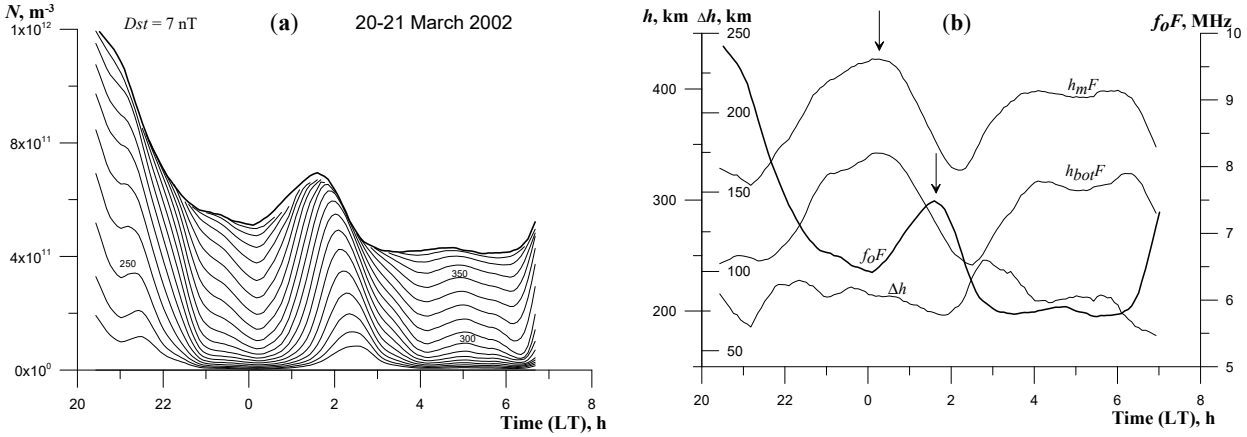

Figure 2. Variations in the electron concentration in time at several fixed heights and in the layer maximum (thick curve) under a low level of magnetic activity, when a post-midnight enhancement in the electron concentration is observed on the background of its quiet diurnal behavior (**a**). The behavior of h_mF, $h_{bot}F$, Δh, and f_oF for this case (**b**).

Figure 2a illustrates the behavior of the electron concentration at a number of fixed heights and at the layer maximum (thick curve) at a very low level of magnetic activity (Dst = 7 nT), at which the probability of generating a high-amplitude LSTID is almost zero. The distance between adjacent heights is 10 km, and the lower height for this case is 230 km. Figure 2b illustrates the behavior of h_mF, $h_{bot}F$, Δh and f_0F. Comparing the time behavior of the parameters of the nighttime enhancement, one can see that its characteristic features completely repeat the features described in [12] for the types of ionospheric plasma disturbances mentioned in the introduction.

These features of behavior include the rise of the layer with its subsequent downward movement and simultaneous compression, leading to the formation of the maximum

value of N_mF at the moment of maximum compression (t~01:45). The behavior of the listed parameters of the layer fits into the scheme of the mechanism for the formation of nighttime enhancements in ionization, described in [7]. Let us consider the main points of this mechanism using the example of the enhancement shown in Figure 2. The decrease in the critical frequency at the beginning of the measurement session is due to the switching off of the ionizing radiation of the Sun after its sunset and chemical losses caused by plasma recombination. The rapid enhancement in the electron concentration after 06:00 is due to sunrise. Let us consider the behavior of all layer parameters for the ionization enhancement with the N_mF peak at t~01:45, taking into account the sequence of steps considered in [7], which uses a self-consistent method developed by the authors for obtaining thermospheric parameters from incoherent scatter radar data.

The main idea of the method is to fit the theoretical $N(h)$-profile to the observed profile, and thus obtain a self-consistent set of main aeronomic parameters: neutral composition, neutral temperature, vertical plasma drift, and observed height profiles of electron and ion temperatures. Despite the variety of possibilities for realizing enhancements in N_mF, the authors established the main mechanism for the formation of the peak. At night, there is always a downward flow of O^+ ions and electrons from the plasmasphere into the *F*2-layer. The vertical velocity of the plasma is determined by the altitude gradients of the electron concentration, ion and electron temperatures, as well as the gravitational term and the drift velocity determined by the thermospheric wind. The initial stage of the process is an enhancement in the speed of the meridional equatorward thermospheric wind, which lifts the *F*2-layer and thus leads to an enhancement in h_mF. In Figure 2b, this beginning corresponds to the time t~21:00. The rise of the *F*2-layer reduces the recombination rate, and the corresponding plasma loss factor becomes small. In this case, even a moderate plasmaspheric flow is sufficient to start an enhancement in the electron concentration in the *F*2-layer (t~00:00).

An enhancement in the electron concentration leads to a decrease in the electron temperature in the *F*2-layer. A decrease in the electron temperature leads to a decrease in the half-thickness (Δh), and a rapid and further enhancement in the downward flow velocity. An enhancement in the downward velocity of the plasma provides additional plasma inflow into the F2-layer, leading to an enhancement in the electron concentration, etc. This self-sustaining avalanche-like process forms a peak in N_mF at t~01:45. The process stops when the thermospheric wind starts to decrease as the height of the h_mF layer decreases. The layer returns back to the heights where recombination is high, while N_mF begins to decrease and the described process reverses. The maximum flux strictly corresponds to the time of the peak in the N_mF variations, since it is proportional to the product of the velocity and N_mF, and they are maximum around this time. According to this mechanism, there must always be a delay in the peak in N_mF variations relative to the peak in h_mF. The peak in N_mF should form in the region of the h_mF decline.

3.3. Altitude Profiles of LSTID Amplitudes and Nighttime Enhancements

In the previous sections, we studied two types of ionospheric disturbances characterized by different physical mechanisms of their generation. The sources of ionospheric variability listed above demonstrate similar reactions of the ionosphere associated with the temporal expansion and upward rise of the *F*2-layer and its fall, accompanied by its compression, giving a N_mF peak at the moment of maximum compression. In this section, the height profiles of the disturbance amplitudes are compared. To study the height profiles of the LSTID amplitudes for the period 2000–2008 observation sessions were selected, during which perturbations with the relative amplitude (Δh) exceeding 25% were recorded at a height corresponding to A_m. Here, $\Delta_h = A(h)/N(h)$, where $A(h)$ is the absolute wave amplitude at the height h and $N(h)$ is the unperturbed electron concentration at the given height. The selection of observation sessions, during which LSTIDs with large absolute and relative amplitudes were recorded, ensured high accuracy in constructing altitude profiles of amplitudes even near the heights of the layer bottom, which are characterized

by small values of $A(h)$ and $N(h)$. There were 63 such sessions in total. Figure 3a illustrates an example of variations in the electron concentration $N(t)$ for the night of 30–31 August 2004 at a series of heights with a distance between adjacent heights of 10 km. The lower curve corresponds to the height of the bottom of the layer (h = 190 km).

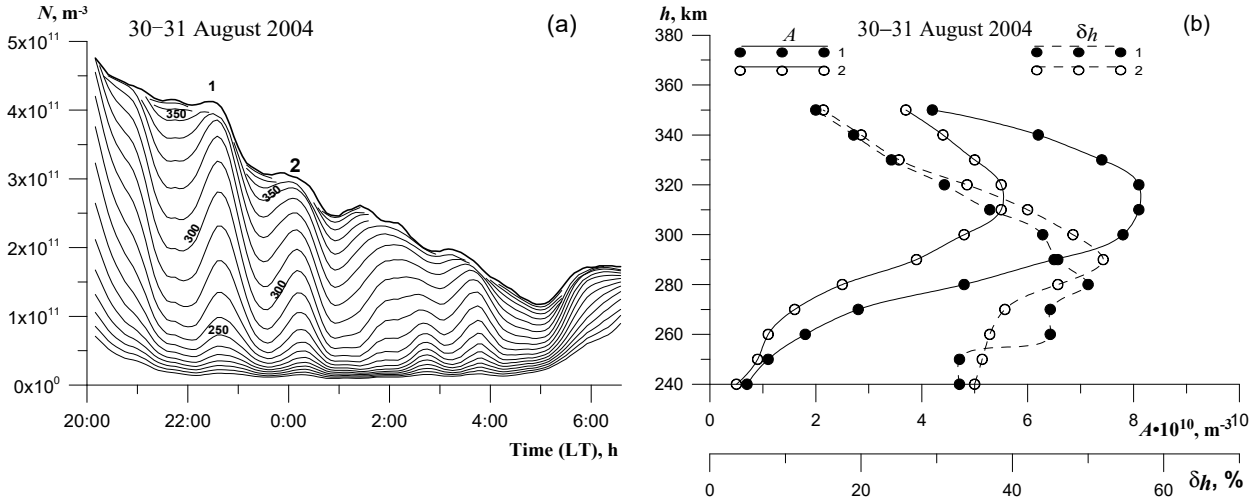

Figure 3. Variations of the electron concentration $N(t)$ for the night of 30–31 August 2004 at a series of heights with a distance between adjacent heights of 10 km (**a**) and the corresponding height profiles of the absolute (solid lines) and relative (dashed lines) disturbance amplitudes 1st wave (dots) and 2nd wave (circles) during the passage of the LSTIDs (**b**).

The upper (thick) curve corresponds to variations in N_mF at the maximum of the $F2$-layer. The figure illustrates smoothed concentration variations with filtered high-frequency fluctuations. The electron concentration variations shown in the figure demonstrate a feature characteristic of most sessions in which LSTIDs were observed. The peculiarity is that the LSTIDs in the $N_mF(t)$ variations manifest themselves much weaker than in the $N(t)$ variations at fixed heights located below the height of the layer maximum. The reasons for such a height dependence of the ionospheric response to the passage of AGWs are considered in [15]. The reason for this phenomenon is the difference in the physical mechanisms that determine the magnitude of the amplitudes. If the magnitude of the variation amplitude N(t) at a fixed height is determined by the mean value and vertical gradient of the electron concentration at this height, then the amplitude at the maximum of the layer whose height does not remain constant but experiences periodic variations is determined by the value of the amplitude of the layer half-thickness variations, which, in turn, is determined by the height gradient of the AGW amplitude.

As noted in [17], in the limiting case, in the absence of a vertical amplitude gradient, when the $F2$-layer oscillates in height without changing its shape, the amplitude of the critical frequency variation becomes equal to zero. Figure 3b illustrates the height profiles of the absolute and relative amplitudes of disturbances 1, 2, calculated from the variations of $N(t)$. Altitude profiles of the disturbance amplitudes were plotted for each periodic wave recorded during the measurement session. In Figure 3a, two waves are clearly visible, which are indicated by the numbers 1 and 2. In this observation session, the heights corresponding to the maximum absolute amplitude, both for wave 1 and for wave 2, were 310–320 km, while the average height of the layer maximum was 370 km. It can be seen that the profiles for waves 1 and 2 differ for both relative and absolute amplitudes. A common property for the waves presented in Figure 3 and for all other analyzed sessions is that the heights corresponding to the maximum values of the absolute amplitudes exceed the heights corresponding to the maximum values of the relative amplitudes. At the same time, the interval of changes in the heights of the maximum profiles for the entire array of analyzed sessions is very wide.

Figure 4 illustrates an example of the behavior of the parameters of the nighttime *F*2-layer, which represents the sequence of the first (t~20:40–22:25) and the second (t~23:10–02:00) enhancements in the electron concentration. The drop in the electron concentration at the beginning of the measurement session is due to the switching off of the ionizing radiation of the Sun after its sunset and chemical losses due to plasma recombination. The rapid increase in the electron concentration in the morning after 06:00 is due to sunrise. The behavior of the electron concentration at a number of fixed heights makes it possible to obtain the height dependence (profile) of the enhancement peak-to-peak value. Here, by the term peak-to-peak value, we mean the difference in electron concentrations at the enhancement maximum (t = 22:30) and at the beginning of the enhancement (t = 20:40).

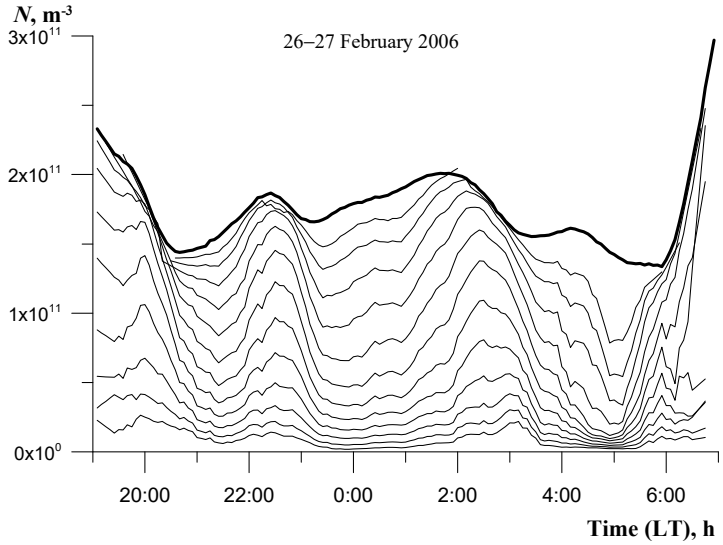

Figure 4. Behavior of the electron concentration of the *F*2-layer at a number of fixed heights during the formation of nighttime enhancements in the electron concentration.

Figure 5 illustrates the height profiles of the enhancement peak-to-peak value for the first (a) and second (b) enhancement and the $N(h)$-profiles for the beginning and end of the enhancements, calculated from the variations of $N(t)$ shown in Figure 4. In the measurement session shown in Figure 4, the height corresponding to the maximum peak-to-peak value, both for the 1st and for the 2nd enhancement, turned out to be 260 km. An analysis of the entire volume of observations showed that those considered in Figure 4 features are preserved during the formation of enhancements and on other dates falling on different seasons and years under different levels of solar activity.

For a quantitative analysis of the parameters of nighttime enhancements, we selected 20 nights characterized by low magnetic activity (Dst > −50 nT) and pronounced manifestations of nighttime enhancements.

Figure 6a is a scatterplot between the height h_{Am} corresponding to the maximum peak-to-peak value and the height of the maximum h_mF of the layer. The interval of heights at which the maximum peak-to-peak value was observed for the entire array of analyzed sessions turned out to be very wide. The regression line calculated by the least squares method is shown as a solid line. The expression for this line and the value of the correlation coefficient r = 0.9 are presented at the top of the figure. It follows from the figure that the difference between h_{Am} and h_mF increases linearly with h_mF. If for h_mF = 280 km the difference is ~38 km, then for h_mF = 380 km the difference is ~54 km. A similar behavior of the height corresponding to the maximum amplitude was also obtained for plasma perturbations generated by the LSTIDs (Figure 6b).

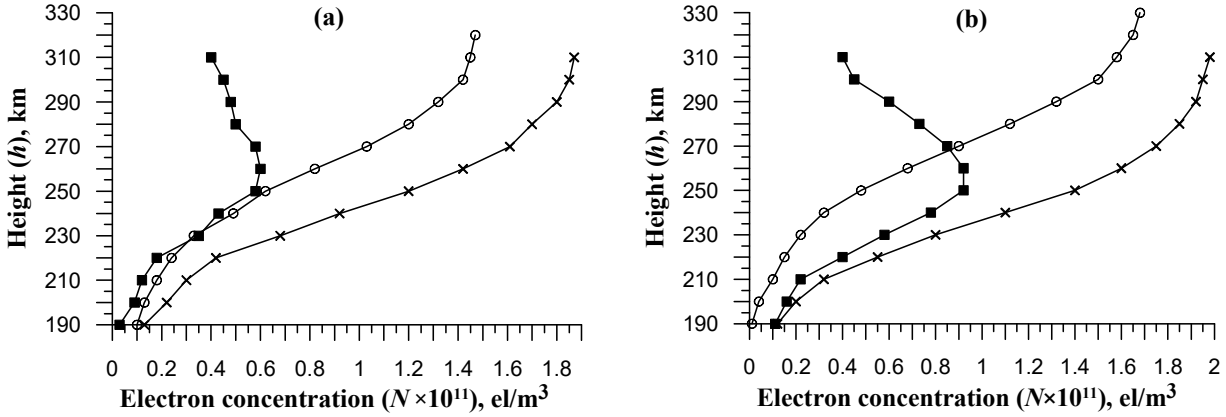

Figure 5. Height profiles of the enhancement peak-to-peak value (■) and $N(h)$-profiles for the beginning (o) and end (x) of the enhancements that took place on 26–27 February 2006 (**a**)—the first enhancement (t_{begin}~20:40, t_{fin}~22:25); (**b**)—the second enhancement (t_{begin}~23:10, t_{fin}~02:00).

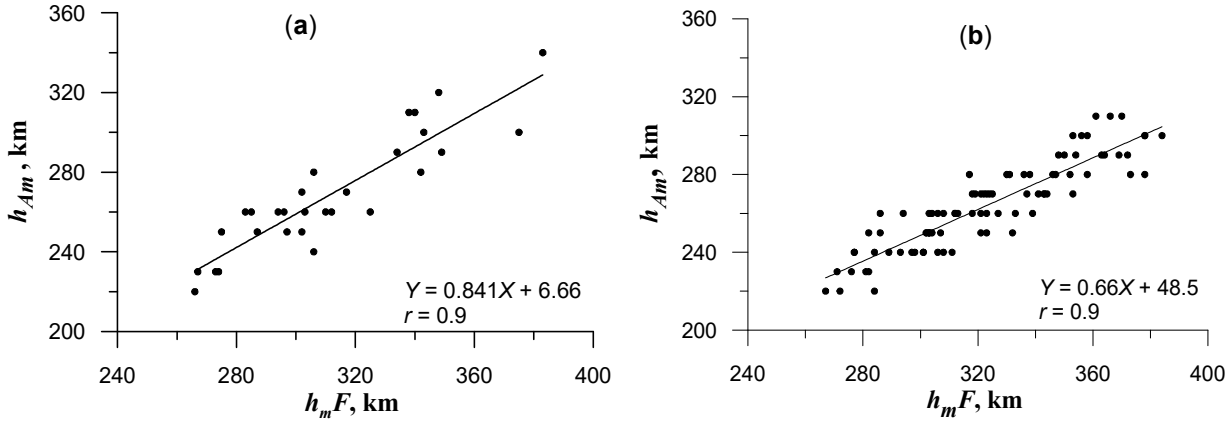

Figure 6. Scatterplot between heights h_{Am} and h_mF obtained over the entire array of analyzed data for nighttime enhancements (**a**) and LSTIDs (**b**).

It can be seen that h_{Am} is always below h_mF, there is a good correlation between h_{Am} and h_mF, the average distance between heights varies from ~45 km for h_mF = 280 km to ~80 km for h_mF = 380 km under low magnetic activity.

Thus, it is shown that two types of ionospheric variations also manifest themselves in the same way in the height profile of the variation amplitudes.

4. Conclusions

Based on the data of vertical sounding of the ionosphere in Almaty in 2000–2008, the paper investigates the response of the *F*2-layer to the passage of large-scale traveling ionospheric disturbances and the formation of nighttime enhancements in the electron concentration. For these two types of disturbances, we compared the time behavior of a number of layer parameters, which demonstrate similar behavior associated with the expansion and upward rise of the ionospheric layer and the downward motion, accompanied by layer compression, giving a N_mF peak at the moment of maximum compression. The height profiles of the enhancement peak-to-peak value in the electron concentration of the *F*2-layer were also obtained, and they were compared with the height profiles of the LSTID amplitudes.

The scatterplots between the height h_{Am} corresponding to the maximum enhancement peak-to-peak value and the height of the maximum h_mF of the layer are calculated. Similar diagrams are calculated for the LSTID amplitudes. The common features of the profiles

of two types of disturbances are shown: h_{Am} is always below h_mF, and there is a good correlation between h_{Am} and h_mF. A similar behavior of the height corresponding to the maximum amplitudes was also obtained for plasma perturbations generated by LSTIDs.

Author Contributions: A.F.Y. conceived, designed and performed the evaluation, and wrote the manuscript. G.I.G. guided the current research work and corrected the manuscript. O.N.K. and Y.G.L. collected the data related to the research and prepared the tables and figures. All authors have read and agreed to the published version of the manuscript.

Funding: This research was financially supported by the Science Committee of the Ministry of Education and Science of the Republic of Kazakhstan (Nur-Sultan, Kazakhstan) (Grant No. AP08855916), the Aerospace Committee of the Ministry of Digital Development, Innovations and Aerospace of the Republic of Kazakhstan (Nur-Sultan, Kazakhstan) (Project BR11265408 Industry (Research)), and by the Science Committee of the Ministry of Education and Science of the Republic of Kazakhstan (Nur-Sultan, Kazakhstan) (Grant No. AP09259375).

Institutional Review Board Statement: Not applicable.

Informed Consent Statement: Not applicable.

Data Availability Statement: Not applicable here.

Conflicts of Interest: The authors declare no conflict of interest.

References

1. Hunsucker, R.D. Atmospheric gravity waves generated in the high latitude ionosphere: A review. *Rev. Geophys.* **1982**, *20*, 293–315. [CrossRef]
2. Vadas, S.L.; Liu, H. Generation of large scale gravity waves and neutral winds in the thermosphere from the dissipation of convectively generated gravity waves. *J. Geophys. Res.* **2009**, *114*, A10310. [CrossRef]
3. Hocke, K.; Schlegel, K. A review of atmospheric gravity waves and traveling ionospheric disturbances: 1982–1995. *Ann. Geophysicae* **1996**, *14*, 917–940.
4. Farelo, A.F.; Herrais, M.; Mikhailov, A.V. Global morphology of nighttime *NmF*2 enhancements. *Ann. Geophys.* **2002**, *20*, 1795–1806. [CrossRef]
5. Bailey, G.J.; Sellek, R.; Balan, N. The effect of interhemispheric coupling on nighttime enhancement in ionospheric total electron content winter at solar minimum. *Ann. Geophys.* **1991**, *9*, 738–747.
6. Mikhailov, A.V.; Leschinskaya, T.Y.; Förster, M. Morphology of *NmF*2 nighttime increases in the Eurasian sector. *Ann. Geophys.* **2000**, *18*, 618–628. [CrossRef]
7. Mikhailov, A.V.; Förster, M.; Leschinskaya, T.Y. On the mechanism of the postmidnight winter *NmF*2 enhancements: Dependence on solar activity. *Ann. Geophys.* **2000**, *18*, 1422–1434. [CrossRef]
8. Pavlov, A.V.; Pavlova, N.M. Mechanism of the postmidnight winter nighttime enhancement in the *NmF*2 over Millstone Hill during 14–17 January 1986. *J. Atmos. Solar-Terr. Phys.* **2005**, *67*, 381–395. [CrossRef]
9. Mikhailov, A.V.; Depueva, A.K.; Leschinskaya, T.Y. Morphology of quiet time *F*2-layer disturbances: High to lower latitudes. *Geomagn. Aeron.* **2004**, *5*, GI1006. [CrossRef]
10. Depuev, V.H.; Depueva, A.H. Reaction of the critical frequency of the *F*2 layer to a sharp depletion in atmospheric pressure. *Geomagn. Aeron.* **2010**, *50*, 804–813. [CrossRef]
11. Yakovets, A.F.; Vodyannikov, V.V.; Andreev, A.B.; Gordienko, G.I.; Litvinov, Y.G. Features of statistical distributions of largescale traveling ionospheric disturbances over Almaty. *Geomagn. Aeron.* **2011**, *51*, 640–645. [CrossRef]
12. Lynn, K.J.W.; Gardiner-Garden, R.S.; Heitmann, A. The observed compression and expansion of the *F*2 ionosphere as a major component of ionospheric variability. *Radio Sci.* **2016**, *51*, 538–552. [CrossRef]
13. Lynn, K.J.W.; Gardiner-Garden, R.S.; Heitmann, A. The spatial and temporal structure of twin peaks and midday bite out in *foF*2 (with associated height changes) in the Australian and South Pacific low midlatitude ionosphere. *J. Geophys. Res. Space Phys.* **2014**, *119*, 10.294–10.304. [CrossRef]
14. Titheridge, J.E. *Ionogram Analysis with the Generalized Program POLAN*; National Data Center: Boulder, CO, USA, 1985; 189p.
15. Yakovets, A.F.; Vodyannikov, V.V.; Gordienko, G.I.; Ashkaliev, Y.F.; Litvinov, Y.G.; Akasov, S.B. Response of the nighttime midlatitude ionosphere to the passage of an atmospheric gravity wave. *Geomagn. Aeron.* **2008**, *48*, 511–517. [CrossRef]
16. Millward, G.H.; Moffett, R.J.; Quegan, S.; Fuller-Rowell, T.J. Effects of an atmospheric gravity wave on the midlatitude ionospheric *F* layer. *J. Geophys. Res.* **1993**, *98*, 19173–19179. [CrossRef]
17. Smertin, V.M.; Namgaladze, A.A. The difference of reactions of the ionospheric *F*2-region to the effect of internal gravity waves under daytime and nighttime conditions. *Radiofizika* **1982**, *5*, 577–579. (In Russian)